Plasmonics of magnetic and topological graphene-based nanostructures

Dmitry Kuzmin, Igor Bychkov, Vladimir Shavrov, Vasily Temnov

Review article

Dmitry A. Kuzmin*, Igor V. Bychkov, Vladimir G. Shavrov and Vasily V. Temnov*

Plasmonics of magnetic and topological graphene-based nanostructures

https://doi.org/10.1515/nanoph-2017-0095
Received September 19, 2017; revised November 10, 2017; accepted November 29, 2017

Abstract: Graphene is a unique material in the study of the fundamental limits of plasmonics. Apart from the ultimate single-layer thickness, its carrier concentration can be tuned by chemical doping or applying an electric field. In this manner, the electrodynamic properties of graphene can be varied from highly conductive to dielectric. Graphene supports strongly confined, propagating surface plasmon polaritons (SPPs) in a broad spectral range from terahertz to mid-infrared frequencies. It also possesses a strong magneto-optical response and thus provides complimentary architectures to conventional magneto-plasmonics based on magneto-optically active metals or dielectrics. Despite a large number of review articles devoted to plasmonic properties and applications of graphene, little is known about graphene magneto-plasmonics and topological effects in graphene-based nanostructures, which represent the main subject of this review. We discuss several strategies to enhance plasmonic effects in topologically distinct closed surface landscapes, i.e. graphene nanotubes, cylindrical nanocavities and toroidal nanostructures. A novel phenomenon of the strongly asymmetric SPP propagation on chiral meta-structures and the fundamental relations between structural and plasmonic topological indices are reviewed.

Keywords: graphene; inverse magneto-optical effects; magneto-optical Faraday effect; magneto-plasmonics; surface plasmon polaritons.

***Corresponding authors: Dmitry A. Kuzmin,** Chelyabinsk State University, Department of Radio-Physics and Electronics, Br. Kashirinykh Street 129, 454001 Chelyabinsk, Russian Federation; and South Ural State University (National Research University), 76 Lenin Prospekt, Chelyabinsk 454080, Russian Federation, e-mail: kuzminda@csu.ru; and **Vasily V. Temnov,** Institut des Molécules et Matériaux du Mans, CNRS UMR 6283, Université du Maine, 72085 Le Mans Cedex, France; and Groupe d'Etude de la Matiere Condensée (GEMaC), Université de Versailles-Saint Quentin en Yvelines, CNRS UMR 8635, Université Paris-Sacley, 45 avenue des Etats-Unis, 78035 Versailles Cedex, France, e-mail: vasily.temnov@univ-lemans.fr
Igor V. Bychkov: Chelyabinsk State University, Department of Radio-Physics and Electronics, Br. Kashirinykh Street 129, 454001 Chelyabinsk, Russian Federation; and South Ural State University (National Research University), 76 Lenin Prospekt, Chelyabinsk 454080, Russian Federation
Vladimir G. Shavrov: Kotelnikov Institute of Radio-engineering and Electronics of RAS, 11/7 Mokhovaya Street, Moscow 125009, Russian Federation

1 Introduction

Graphene opens up wide prospects for numerous flatland photonic and plasmonic applications [1–7]. Graphene-based waveguides support localized electromagnetic surface plasmon polariton (SPP) waves, both TE and TM polarized [8–16]. Their tight confinement and long propagation length allow for observing strong light-matter interactions in graphene-based structures [17]. Optical properties of graphene can be controlled by a number of external parameters such as electrostatic bias, magnetic field or chemical doping.

To realize any plasmonic device, one should possess a tool for SPP manipulation. A conventional approach in noble metal-based active plasmonics relies on combining plasmonic and optically active materials [18–22]. For example, the coupling between magnetic and optical properties in magneto-optical materials leads to the optically induced magnetic fields through the inverse Faraday effect [23–26] or enhanced magneto-optical effects due to plasmonic excitations [27–34].

Spatial nanostructuring of graphene offers another unique playground known as plasmonic meta-surfaces. A periodic arrangement of densely packed subwavelength graphene stripes forms a meta-surface (see Figure 1A), which has a lot of promising plasmonic properties: it can generally support both elliptic (Figure 1B) and hyperbolic SPPs (Figure 1C) depending on various parameters such as structure periodicity, its filling factor, graphene Fermi energy and frequency of exciting light [35–37]. In the hyperbolic regime, enhanced light-matter interactions are

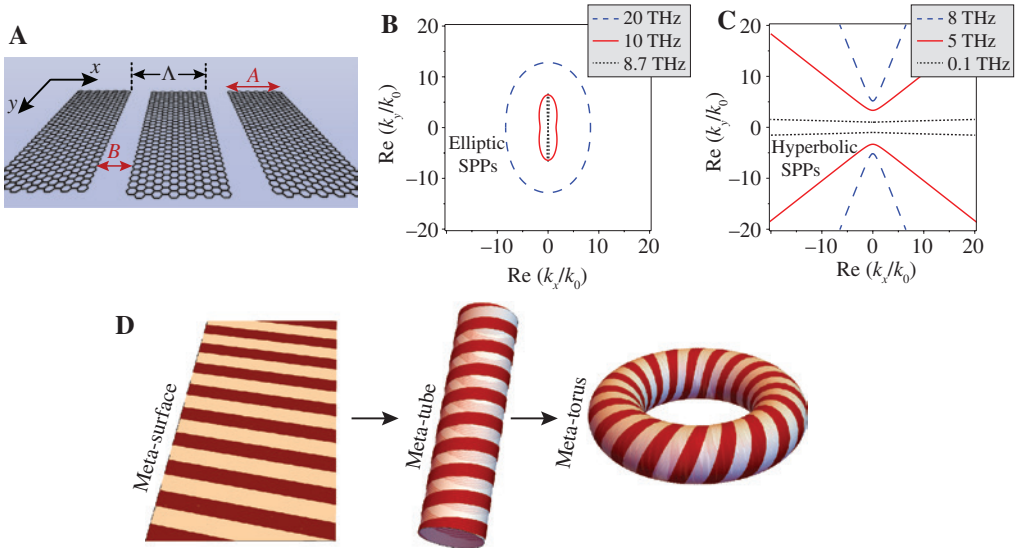

Figure 1: Plasmonic meta-surfaces and topological nanostructures.
(A) An array of densely packed graphene stripes with subwavelength periodicity Λ forms a metasurface that may support both elliptic (B) and hyperbolic SPPs (C). A rolled-up meta-surface forms a meta-tube, and its donut-like shape is a meta-torus (D). In B and C, Λ = 50 nm, A = 45 nm, B = 5 nm.

possible because of the strong spatial confinement of SPP electric field.

The intrinsic topological character (elliptic versus hyperbolic) of SPP dispersion on a meta-surface can be changed, for a given frequency, by tuning the optical properties through the highly anisotropic "epsilon-near-zero points", for example by using an external electric bias voltage [35–37]. This property is of great interest for the controlled guiding of SPPs.

Another way to merge topology with graphene plasmonics (and nanophotonics in general) is to create topologically distinct 3D objects formed by 2D meta-surfaces. Rolling up a meta-surface in a tube forms a meta-tube and bending the latter into the torus forms what we denote as a meta-torus (Figure 1D). As we are going to show in this review, these geometrical transformations give rise to distinct topological indices, which largely determine the properties of plasmonic modes. The interplay of the intrinsic (elliptic versus hyperbolic) topology of SPPs propagating on a flat 2D meta-surface and the geometrical 3D topology of nanostructures can induce novel plasmonic effects: a giant azimuthal rotation of intensity distribution of particular SPP modes upon propagation, one-way propagation of SPPs, vanishing of the Fabry-Perot resonances in finite length meta-tubes, unidirectional circulating Mach-Zehnder-like resonances in a meta-torus, etc.

The cylindrical geometry deserves particular attention as it provides a common basis for plasmonics in chiral media [38–42] and non-reciprocal magneto-optics in waveguides. It is known that the parallel external magnetic field can rotate a spatially inhomogeneous intensity distribution (i.e. speckle-pattern) of light in the cross-section plane upon its propagation along an optical fiber [43–46]. Recently, we have demonstrated that in graphene-coated optical fibers (with magneto-optical fiber material), one can control such a rotation by an external magnetic field. However, for an observable rotation, it is necessary to have a fiber length of a few centimeters [47]. In line with the general trend of enhancing of the magneto-optical effects in magneto-plasmonic nanostructures, it has been shown that the above-mentioned rotation can be drastically enhanced in graphene-coated gyrotropic nanowires [48] because of the reduction of the wire radius results in a stronger confinement and increase of the wave vector of SPP modes. The magneto-optical effects in gyrotropic cylindrical structures have been investigated within the framework of the electromagnetic scattering problem [49, 50] and led to numerous applications in physics of optical devices [51–53]. Recent plasmonic experiments performed on uniformly sized arrays of carbon nanotubes [54], which represent an ultimate size limit of nanoscaled graphene nanowires, are worth mentioning.

The above-mentioned effects on cylindrical geometry originate from the magnetic symmetry breaking for the azimuthal modes rotating in the opposite directions (i.e. with opposite signs of the azimuthal mode index m, or the so-called topological charge). An alternative way to introduce symmetry breaking is provided by the chirality.

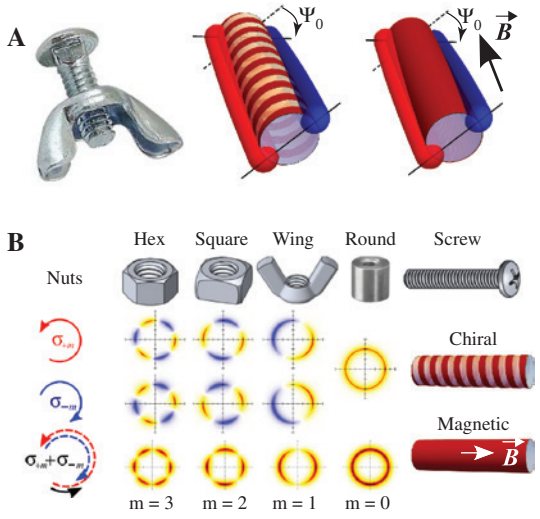

Figure 2: Structural and electromagnetic chirality of functional nanowires.
(A) Similar to a nut on a screw, the spatially inhomogeneous azimuthal SPP intensity distribution (speckle pattern) rotates upon propagation along both chiral and magneto-optical graphene-based nanowires. (B) Chiral σ_{+m} and σ_{-m} SPP modes characterized by opposite azimuthal indices $\pm m$ propagate along plasmonic nanowires with different k-vectors resulting in the asymmetry in the rotation of their electric field distribution upon propagation per unit length. More complex superpositions (speckle pattern) composed of several modes, like $\sigma_{+m}+\sigma_{-m}$, rotate upon propagation as well. The symmetry breaking between the chiral $\pm m$ SPP modes can be due to either the chirality in a graphene meta-tube or the magneto-optical activity of a dielectric core in a graphene-coated nanowire.

Chirality, which does not exist on flat surfaces, can be introduced in a twisted bilayer graphene [55, 56] or by winding up a flat graphene-based meta-surface in a cylindrical meta-tube [57].

The intuitive picture of the aforementioned effects is illustrated in Figure 2. Chiral, azimuthal plasmonic modes propagating along the cylindrical structures are somewhat analogous to the nuts on the screws (Figure 2A). Higher-order plasmonic modes possess $2m$ nodes, which makes the angular intensity distribution visually resembling the shape of common nuts (Figure 2B). Although in the mechanical case, the rotation direction of the nut is determined by the (left- or right-handed) thread on the screw; in plasmonics, both rotation directions are generally possible giving rise to the propagating electromagnetic modes rotating clockwise ($+m$) or counterclockwise ($-m$). However, under appropriate conditions, in analogy to the mechanical nut-on-the-screw example, the chirality of the propagating plasmonic modes is dictated by the chirality of the meta-tube or by the direction of the magnetic field, and modes with the opposite chirality cannot propagate.

A linear superposition of azimuthal σ_{+m} and σ_{-m} modes creates a spatially inhomogeneous intensity distribution (speckle pattern) which is slowly rotating upon propagation along the wire due to the slightly different wave vectors for σ_{+m} and σ_{-m} modes. Figure 2 illustrates that the $\sigma_{+m}+\sigma_{-m}$ superposition of SPP modes rotates similarly on a chiral meta-tube and a graphene-coated magneto-optical nanowire.

In the following, we review the optical, magneto-optical and magneto-plasmonic properties of graphene, plasmonics of graphene-based meta-surfaces, magneto-plasmonics of graphene-based cylinders and novel plasmonic effects in topological graphene-based nanostructures. We believe that these results extend beyond the graphene plasmonics as they are qualitatively valid for arbitrary nanostructures formed by artificial 2D meta-surfaces supporting the propagating SPP modes.

2 Optical and magneto-optical properties of graphene

Dirac's character of quasiparticles in graphene leads to unusual dynamics of the electrons and holes. For example, the unconventional quantum Hall effect has been predicted theoretically [58–63] and observed experimentally [64–66]. Another feature is a finite effective cyclotron mass for the massless Dirac quasiparticles in both electric and magnetic dc measurements which was found to vary as a square root of the number of carriers [64, 67–69]. From the experimental measurement of the graphene transmittance spectra [70–72], the dynamical conductivity was found to be frequency independent for the visible light $\sigma(\omega)=e^2/4\hbar$, which is in agreement with theoretical calculations [73–75].

From the point of view of theory, graphene is commonly described in terms of Dirac's gapless fermions. According to this picture, in graphene, there are two bands at the **K** hexagon vertices of the Brillouin zone without any gap between them, and the electron dispersion can be considered as linear in the wide wave vector region. Summing up the contributions of these points, i.e. integrating over the angle of the two-dimensional momentum vector **p** leads to the general quantum expression for the dynamic conductivity of graphene depending on both the frequency ω and the wave vector k [76, 77] and meaning that both temporal and spatial dispersion should be taken into account. In the optical range, one can neglect the spatial dispersion of conductivity. This conductivity represents a sum of two contributions $\sigma(\omega)=\sigma_{\text{intra}}(\omega)+\sigma_{\text{inter}}(\omega)$.

The first term $\sigma_{intra}(\omega)$, corresponding to the intraband electron-phonon scattering process, has a Drude-like behavior in the high-frequency regime $\omega \gg \max(kv_F, \tau^{-1})$ [76–79], where v_F is the carrier's velocity (Fermi velocity) and τ is the carrier's relaxation time:

$$\sigma_{intra}(\omega) = \frac{2ie^2 k_B T \ln[2\cosh(\mu_{ch}/2k_BT)]}{\pi\hbar(\omega + i\tau^{-1})} \xrightarrow{\mu_{ch} \gg k_BT} \frac{ie^2|\mu_{ch}|}{\pi\hbar(\omega + i\tau^{-1})}, \quad (1)$$

whereas the second one, $\sigma_{inter}(\omega)$, corresponds to the direct interband electron transitions and plays the leading role around the absorption edge $\hbar\omega \approx 2\mu_{ch}$:

$$\sigma_{inter}(\omega) = \frac{e^2}{4\hbar}\left\{\frac{1}{2} + \frac{1}{\pi}\arctan\left[\frac{\hbar\omega - 2\mu_{ch}}{2k_BT}\right] - \frac{i}{2\pi}\ln\frac{(\hbar\omega + 2\mu_{ch})^2}{(\hbar\omega - 2\mu_{ch})^2 + (2k_BT)^2}\right\}. \quad (2)$$

For room temperature $k_BT \sim 25$ meV, for THz, near-infrared and visible frequencies, the photon energies are ~5 meV, 1 eV and 2.5 eV, respectively. For high-quality graphene, the relaxation time at room temperature is about 0.1 ps [80], which corresponds to the energy scale $\Gamma = \hbar/\tau \sim 5$ meV. The graphene chemical potential (or Fermi energy) $\mu_{ch} \approx \hbar v_F(\pi n)^{1/2}$ is determined by surface carrier density n and Fermi velocity $v_F \approx 10^6$ m/s. For example, $n \approx 8 \times 10^{13}$ cm^{-2} corresponds to $\mu_{ch} \approx 1$ eV. We should note that the above-mentioned equations assume the electron's dispersion to be linear. This requires the length of the electron's wave vectors at the Fermi level to be relatively small (typically less than 10^8 cm^{-1}), as compared with the size of the Brillouin zone. This condition is satisfied for small carrier concentration $n \ll 10^{16}$ cm^{-2}. Similar estimates show that for graphene's chemical potential of the order of 1 eV, the electron's dispersion is also linear and the above expressions are applicable.

Moreover, the electromagnetic response of graphene at terahertz frequencies and the commonly used 0.3–1 eV range of chemical potential is dominated by a simple Drude-like intraband conductivity and the interband contribution can be neglected. In contrast, at the near-infrared and visible frequencies, the interband term plays the crucial role. In the first case, the terahertz frequency can match the absorption edge, $\hbar\omega_{THz} \approx 2\mu_{ch}$, whereas in the second (near IR to visible) case, we obtain $\sigma_{intra}(\omega) \to 0$, $\sigma_{inter}(\omega) \to e^2/4\hbar$.

The application of the external magnetic field B leads to the charge carriers' circulation in cyclotron orbits and the famous graphene Dirac cone splits in a discrete set of non-equidistant Landau energy levels (see Figure 3). In contrast to the usual semiconductors and metals with parabolic carriers' dispersion, linear dispersion of graphene's carriers leads to non-equidistant Landau levels ($E_j = [2\hbar v^2 |eB| j]^{1/2}$, where j is the level number) and include a characteristic zero-energy state ($j = 0$). For magneto-optics, the graphene layer has resonant effects at the photon energies equal to the Landau level difference. Another feature is associated with the Hall conductivity of graphene, which leads to the Faraday and Kerr effects.

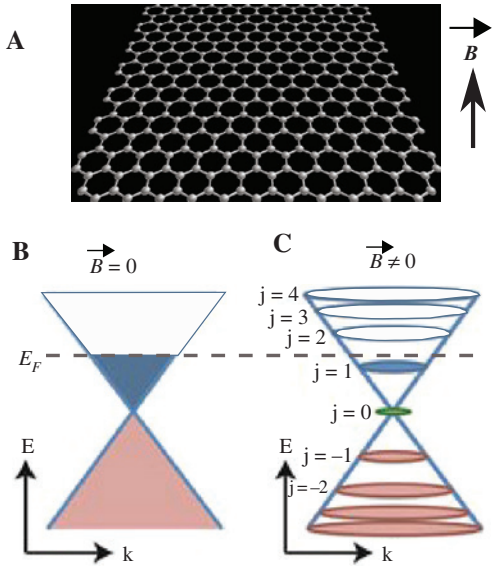

Figure 3: Graphene in an external perpendicular magnetic field (A) has a discrete set of non-equidistant electronic energy levels (Landau levels) in contrast to zero magnetic field (B, C).

Experimental investigations (see Figure 4) have shown that the Faraday rotation in single-layer graphene may reach giant values of 6° in the magnetic field of 7 T in the far-infrared range [81], about 1° in low magnetic fields <0.7 T in the terahertz frequency range [82], and in magnetic fields, <5 T at microwave frequencies relevant for telecommunication, cell phones, wi-fi etc. [83]. The theoretical conductivity tensor of graphene in external magnetic field was calculated in few works [84, 85], and results based on these theories are in good agreement with the experimental data.

The above-mentioned peculiarities of the Faraday rotation may be described by the 2D conductivity tensor with non-zero off-diagonal components. In general case, the analytical expressions for these components are quite cumbersome, but at low enough frequencies (or high doping level) obeying $\hbar\omega \ll 2\mu_{ch}$, low magnetic fields $E_1 \ll 2\mu_{ch}$ and low temperatures $k_BT \ll 2\mu_{ch}$, they reduce to the classical Drude form

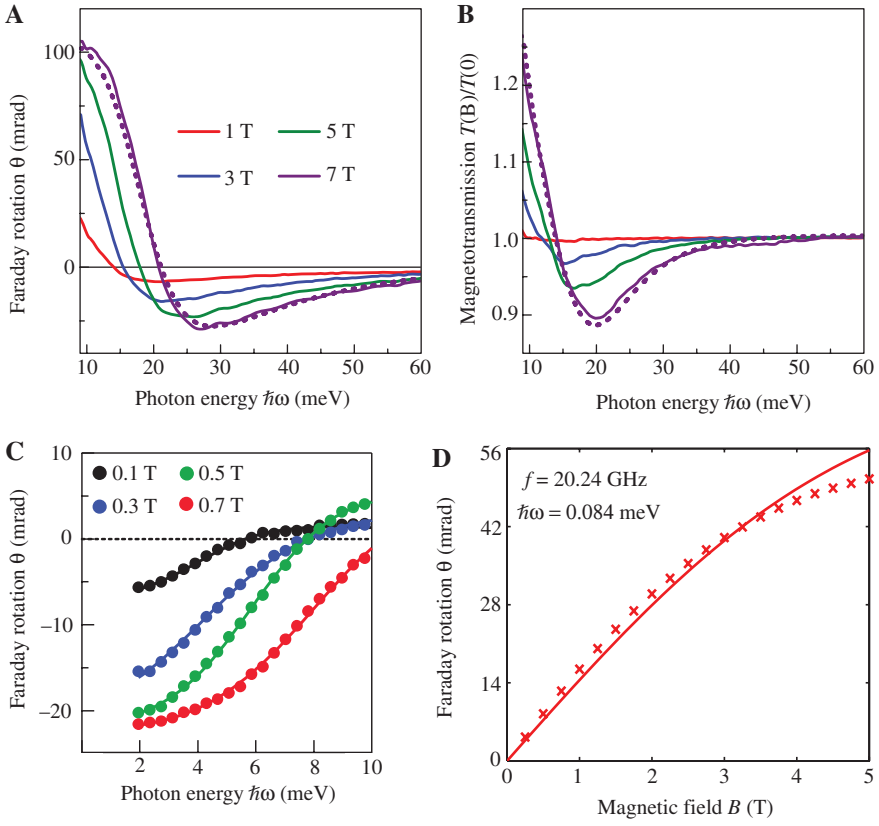

Figure 4: Faraday rotation of single-layer graphene measured at different frequencies and magnetic fields. (A, B) High-frequency and high-magnetic fields (adapted from [81]), (C) lower-frequency and low-magnetic fields (adapted from [82]) and (D) low-frequency and different magnetic fields (adapted from [83]).

$$\hat{\sigma} = \begin{pmatrix} \sigma & -\sigma_H \\ \sigma_H & \sigma \end{pmatrix},$$
$$\sigma = \sigma_0 \frac{1 + i\omega\tau}{(\omega_c\tau)^2 + (1 + i\omega\tau)^2},$$
$$\sigma_H = \sigma_0 \frac{\omega_c\tau}{(\omega_c\tau)^2 + (1 + i\omega\tau)^2}. \quad (3)$$

Here, $\sigma_0 = \sigma_{intra}(\omega)$ is given by Eq. (1) and $\omega_c = v_F(2|eB|/\hbar)^{1/2}$ denotes the cyclotron frequency.

To the best of our knowledge, previous investigations of electronic and optical properties in graphene have been restricted to the perpendicular orientation of the magnetic field, which drastically perturbs the trajectories of the electrons moving on their cyclotron orbits. In another case of an in-plane magnetic field, the magneto-optical effect in graphene is strongly suppressed for a simple reason. The thickness d of graphene monolayer falls within the range 0.1–0.5 nm [12, 14] and the cyclotron radius reads $R_c = mv/eB = \hbar k_F/eB \approx 12(n[10^{10}\ \text{cm}^{-2}])^{1/2}/B[\text{T}]$ nm, $\hbar$ is the Plank constant, n is carrier concentration, k_F is the Fermi wave vector [42]. For carriers concentrations $n \sim 10^{13}$ cm^{-2} and reasonable values of the magnetic field, the cyclotron radius is much larger than graphene thickness: $R_c/d > 10^3/B[\text{T}]$. Therefore, the trajectories of the electrons are almost not perturbed and minor residual magneto-optical effects in graphene do not affect SPP properties. In a quantum-mechanical picture, the quantization of the magnetic flux through such an extremely stretched contour starts playing a role, i.e. the first Landau level emerges also for $B > B_{crit} \sim 10^3$ T.

In a different geometry of a graphene tube placed in a collinear magnetic field, the magneto-optical effects could become important only in a special case when the cyclotron and tube radii become equal. For a tube with the radius $R \sim 200$ nm, it would be the case for $B_{crit} \sim 10$ T.

3 Intrinsic magneto-plasmonics in graphene

The magneto-optical properties of graphene may also give rise to magneto-plasmonics. In contrast to plasmonic

excitations which are usually TM-polarized (i.e. the magnetic component of electromagnetic field is perpendicular to the *k*-vector), magneto-plasmons in graphene are hybrid TM-TE modes (all components of electric and magnetic fields are non-zero).

In magnetically biased single-layer graphene, an ensemble of weakly decaying quasi-TE modes, separated by magneto-plasmon-polariton modes, emerges due to the magnetic field [86–88] (see Figure 5A–D). Magneto-plasmons have been experimentally observed in graphene

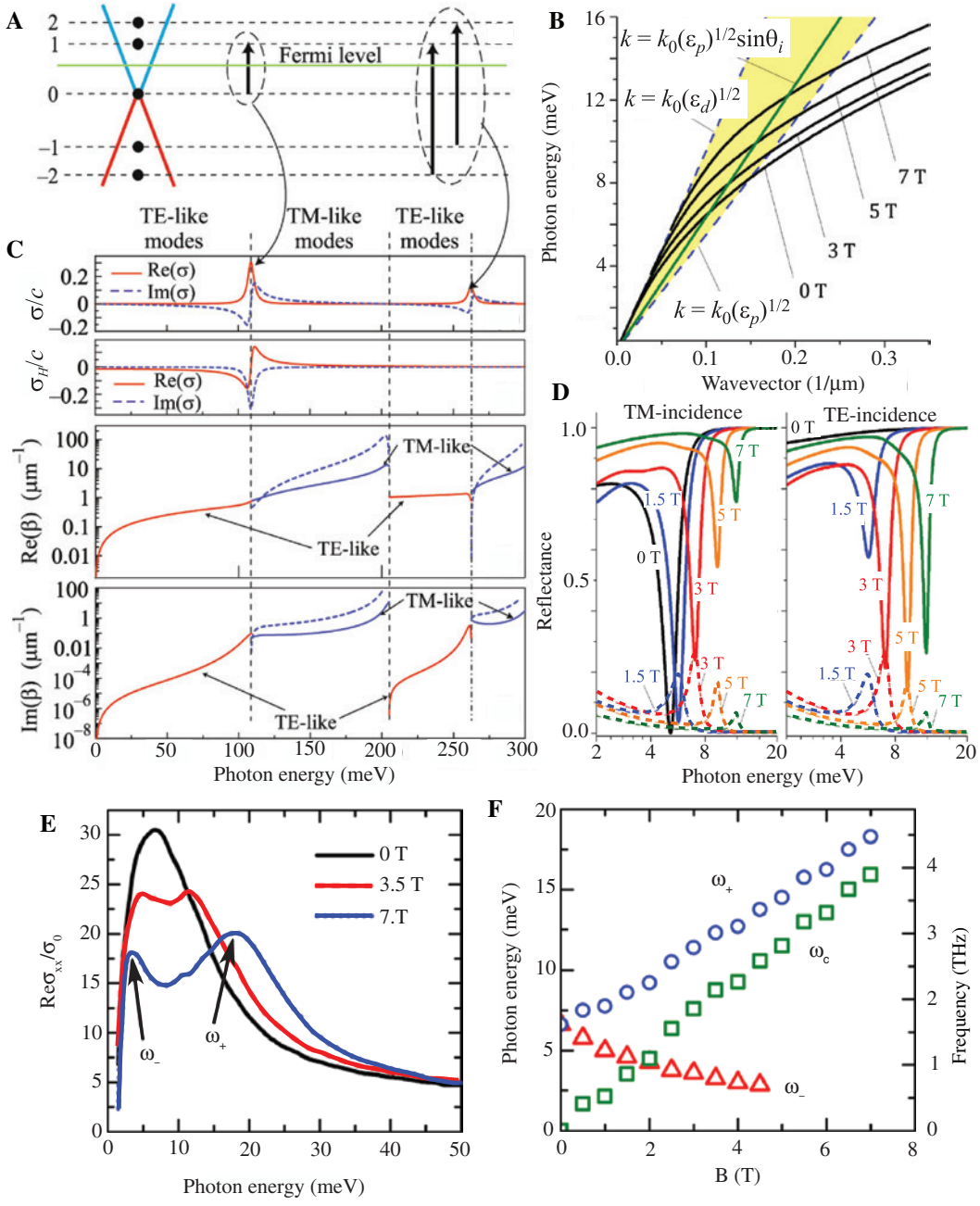

Figure 5: Magneto-plasmons in graphene.
(A) The scheme of Landau levels in graphene. (B, C) dispersion curves of the magneto-plasmon-polaritons for different values of an external magnetic field. (D) Magneto-plasmon-polaritons in magnetically biased graphene in Otto configuration can be excited by both TE and TM incident wave. In the left panel, the incident wave is TM polarized, and the solid (dashed) lines correspond to TM (TE) reflectance. In the right panel, the incident wave is TE polarized, and the solid (dashed) lines correspond to TE (TM) reflectance. (E, F) Magnetically biased graphene disks may support bulk (ω_+) and edge (ω_-) magneto-plasmons (see text for details). Adapted from [87] (A, C), [88] (B, D) and [89] (E, F).

epitaxially grown on SiC [90], and in layered graphene structures, they even display drift instability [91].

In a finite-width graphene stripe, the magneto-plasmon-polaritons propagating in the transverse direction may form standing-wave resonances across the stripe [92]. Such modes are usually called bulk 2D modes of the graphene stripe. The excitation of these magneto-plasmonic modes may significantly affect the magneto-optical response of graphene nanostructures: patterning the uniform graphene layer into graphene stripes array allow the production of the same Faraday rotation at much smaller magnetic fields [93]. The discussed bulk magneto-plasmons and magneto-plasmon-polaritons are intrinsic to extended graphene films where boundary effects are neglected. In finite-size structures, edge effects become important, as they give rise to the so-called edge magneto-plasmons (localized at the edge) and edge magneto-plasmon-polaritons propagating along the edge [94].

A similar situation is observed in magnetically biased graphene disks [89, 95, 96], which support both the bulk (localized across the disk) modes and the edge (confined to disk edge) one (see Figure 5E and F). Interestingly, these modes degenerate in magnetic-free graphene disks, while external magnetic field leads to the splitting of edge and bulk magneto-plasmons.

Magnetic field-induced breaking of the degeneracy of the edge modes suggests straightforward applications of the magnetically biased graphene stripes in non-reciprocal plasmonic devices such as phase shifters [92], couplers [97], plasmonic isolators [98], directional SPPs excitation [99], magnetically tunable focusing in-planar lenses [100] etc.

4 Plasmonics of graphene-based meta-surfaces

As already mentioned before, meta-surfaces are the 2D analogs of 3D metamaterials. They consist of subwavelength-sized building blocks (the so-called meta-atoms) periodically arranged on a surface. Such ultrathin structures are promising for light manipulation at the nanoscale: they display an anomalous reflection, diffraction-free propagation, allow to create optical vortexes, manifest the photonic spin Hall effect and so on.

One of the simplest graphene-based meta-surfaces is formed by graphene stripes with the width A separated by the spacer width B, with subwavelength periodicity $\Lambda = A + B \ll \lambda$ (in electrostatic limit). The optical response of such meta-surface can be described by the highly anisotropic conductivity tensor [35–37]:

$$\hat{\sigma}_{\text{meta}} = \begin{pmatrix} \sigma_{xx} & \sigma_{xy} \\ \sigma_{yx} & \sigma_{yy} \end{pmatrix}, \tag{4}$$

where all tensor components depend on graphene conductivity $\sigma_g = \sigma_{\text{intra}} + \sigma_{\text{inter}}$ with σ_{intra} and σ_{inter} given by Eqs. (1) and (2) and the capacitive coupling $\sigma_C = i\omega\varepsilon_0\varepsilon_{\text{eff}}\Lambda\ln[\sin(\pi B/2\Lambda)]/\pi$ between the stripes. The topological transition from the elliptic to the hyperbolic topology around σ-near-zero case corresponds to $\text{Im}\{A\sigma_C + B\sigma_g\} = 0$. This transition plays a crucial role in plasmonics: whereas in the case of elliptic topology, SPPs can propagate in all directions; in the hyperbolic case, their propagation is allowed in some specific directions only. Physically, the hyperbolic meta-surface displays the metal-like behavior in one direction while showing the dielectric-like response in the orthogonal directions. Due to the pronounced frequency dependence of σ_g and σ_C, the spectral regions of the hyperbolic and elliptic topology are separated by a highly anisotropic σ-near-zero point, where large dissipative losses occur.

Figure 6A shows the conductivity components of the meta-surface with the fixed periodicity 50 nm under the variation of the stripe width. The hyperbolic regime corresponds to the region with the different signs of the σ_{xx} and σ_{yy}. SPPs excited by a point dipole in the meta-surface working in the hyperbolic regime are shown in Figure 6B.

As we discussed in the previous section, the excitation of these magneto-plasmonic modes may significantly influence the magneto-optical response of a patterned graphene layer. Figure 6C demonstrates the influence of periodic patterning of graphene and the large magnetic field on the spectra of Faraday rotation [94]. For an increasing magnetic field, the maxima of the dashed (uniform graphene) and solid (patterned graphene) lines in Figure 6E shift to higher frequencies. The maxima of the patterned graphene are also shifted to higher frequencies as compared to the uniform graphene.

5 Magneto-plasmonics of graphene-based cylindrical structures

The intrinsic magneto-optical activity of graphene is unfortunately useless for cylindrical structures. It needs the static magnetic field to be perpendicular with respect

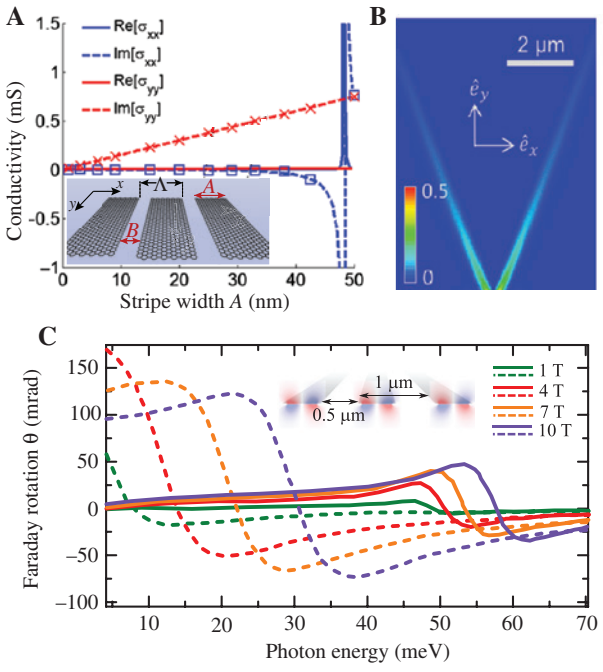

Figure 6: Magneto-plasmonics on graphene meta-surfaces. (A) Effective conductivity of the meta-surface formed by graphene stripes of the width A placed with the periodicity $\Lambda = 50$ nm in long wave limit (i.e. $\lambda_{SPP} \gg \Lambda$). Operating frequency is 10 THz. (B) SPPs excitation by the point source placed near the meta-surface working in hyperbolic regime. Magneto-plasmon-assisted Faraday rotation by a meta-surface placed in a perpendicular external magnetic field (C). Dashed lines correspond to uniform graphene. Adapted from [36] (A, B) and [93] (C).

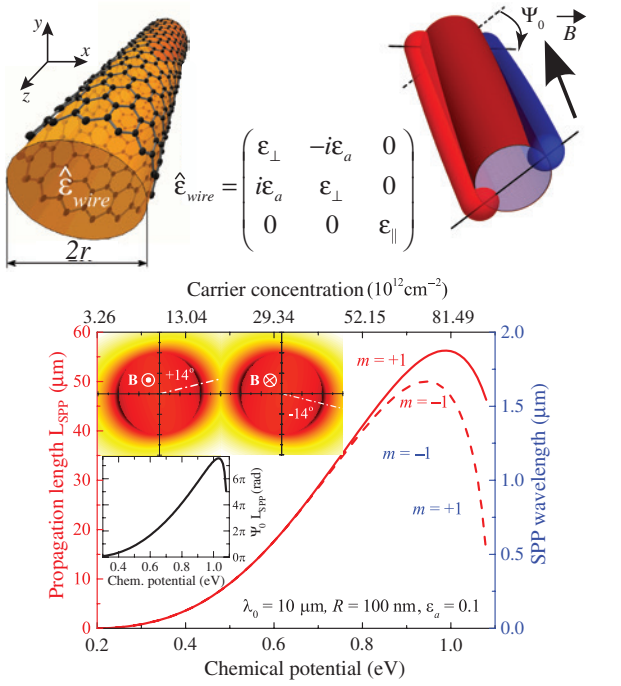

Figure 7: A magneto-optical nanowire covered with a graphene layer supports high-order azimuthal SPP modes with $|m| > 0$. Both the SPP propagation length (left axis) and wavelength (right axis) for the first-order mode with $|m| = 1$ depend on graphene chemical potential (corresponding carrier concentration is shown on the top axis). Core radius $r = 100$ nm, frequency of electromagnetic wave $f = 30$ THz (vacuum wavelength $\lambda_0 = 10$ μm), permittivity of the core $\varepsilon_\perp = \varepsilon_\parallel = 3$, gyration of the core $\varepsilon_a = 0.1$. The outer medium is in vacuum. In the upper inset, the field distributions are shown for the opposite magnetic field directions at $z_0 = 500$ nm and $\mu_{ch} = 1$ eV. Total rotation of the field distribution upon the reversal of the external magnetic field with $\mathbf{B} \approx 1.8$ T (such magnetic field leads to $\varepsilon_a = 0.1$ at Verdet constant $V = 10^4$ rad T^{-1} m^{-1}) pointing along the nanowire axis is about 28°. The lower inset shows the figure of merit, i.e. the rotation angle per propagation length. Adapted from [48].

to graphene. In cylindrical geometry, only the radial magnetic field will satisfy this condition (or at least the magnetic field with the non-zero radial component). Such magnetic fields are hardly obtained in real experimental conditions. It is worth mentioning that plasmonic structures formed by graphene and magneto-active materials have some interesting features in the planar geometry [101, 102]. Thus, to introduce magneto-optical activity into cylindrical graphene-based structures, one may use a magneto-active cylinder covered by graphene. Such a structure has been recently investigated [48] (see Figure 7).

SPP modes propagating on the graphene-covered non-gyrotropic nanowires induce the complex distribution of the stationary magnetic field generated via the inverse Faraday effect [100]. At present, we assume that the SPP intensity is so small that the inverse Faraday effect inside the magnetic nanowire can be neglected. Then, the magneto-active core of the cylinder can be described in the cylindrical coordinate system (ρ, φ, z) by the intensity-independent dielectric permittivity tensor with non-zero off-diagonal components $\varepsilon_{\rho\varphi} = -\varepsilon_{\varphi\rho} = i\varepsilon_a$. The cylindrical geometry leads to the azimuthal and axial field distribution of $\mathbf{E}_m$, $\mathbf{H}_m \sim \exp[ih_m z + im\varphi]$, where $h_m = h'_m + ih''_m$ is a complex SPP wave vector (SPP propagation length is $L_{SPP} = 1/h''_m$ and SPP wavelength $\lambda_{SPP} = 2\pi/h'_m$), m is the azimuthal mode index characterizing SPP's chirality. These chiral, azimuthal SPP modes can be understood as plane electromagnetic waves characterized by the longitudinal (along the nanowire axis) and transverse (along the nanowire surface, perpendicular to the nanowire axis) components of the wave vector $k_\parallel = h_{\pm m}$ and $k_\perp = \pm m/r$, respectively. Therefore, the phase front of the azimuthal SPP modes is tilted with respect to the nanowire axis by an angle α_m obeying $\mathrm{tg}\,\alpha_m = k_\parallel/k_\perp = h_m r/m$. The chiral modes with $|m| > 0$ exist above the cut-off frequency. The number of supported modes at the fixed vacuum wavelength λ_0 can be estimated as $\mathrm{Re}[i2\pi r(\varepsilon_\perp + \varepsilon_0)c/(\sigma_g \lambda_0)]$. An increase in the core permittivity leads to an increase in the number

of supported modes. Whereas for graphene-covered non-gyrotropic nanowires modes with opposite chirality (opposite signs of m) are degenerate [16], these modes propagate along the wire at slightly different velocities in the gyrotropic case.

This effect has a simple practical application as a nanoscaled Faraday isolator. Imagine that we excite a gyrotropic graphene-covered nanowire of length z_0 by a linearly polarized plane electromagnetic wave at one of the tips. Along with a non-chiral $m=0$ mode, a linear superposition of σ_{+1} and σ_{-1} modes will be excited [103]. The azimuthal intensity distribution $\cos[\varphi]$ of this mode superposition will be rotated around the nanowire axis by the angle $\psi = z_0(\mathrm{Re}\{h_-\} - \mathrm{Re}\{h_+\})/2$ and out-coupled into the linearly polarized free-space radiation with the polarization plane rotated by the angle ψ. This polarization rotation is characterized by the specific rotation angle $\psi_0 = \psi/z_0$ per unit length. The maximum rotation $\psi_0 L_{SPP}$ is achieved in the case of the nanowire length equal to the SPP propagation length, $z_0 = L_{SPP}$, and serves as another figure-of-merit in magneto-plasmonics [104].

For the parameters of the nanowire radius, $r=100$ nm (quantum effects in graphene structures should be taken into account for the size of the structure less than ≈20 nm [105]); $\varepsilon_\perp = \varepsilon_\parallel = 3$, at the lower part of the mid-infrared region ($f=30$ THz), only one azimuthally dependent mode can be excited. The characteristics of this mode are shown in Figure 7: the total rotation of the field distribution upon the reversal of the external magnetic field pointing along the nanowire axis at $z=500$ nm and $\mu_{ch}=1$ eV is about 28°. This value is roughly 30 times larger compared to the angle of rotation of the polarization plane for a plane electromagnetic wave travelling in the volume of the magneto-optical material along magnetization direction $2BVz = 1.04°$ for $B \approx 1.8$ T (such magnetic field leads to $\varepsilon_a = 0.1$ at Verdet constant $V = 10^4$ rad T^{-1} m^{-1}). The rotation per SPP propagation length $L_{SPP} \approx 45$ μm may reach a giant value of 8π. The change in the sign of the gyrotropy ε_a (i.e. change in magnetization or magnetic field direction) leads to the opposite rotation of field distribution. A change in graphene conductivity (or its chemical potential) results in a larger difference in propagation constants for modes with opposite signs of $\pm m$. This may be used to adjust the rotation angle similar to the graphene-covered optical fiber [47]. Both the specific rotation angle and rotation angle over the SPP propagation length increase with the growing chemical potential. The specific rotation angle is larger for higher-order modes, whereas the rotation angle over the SPP propagation length displays an opposite behavior due to the smaller propagation length of higher-order modes. For maximum rotation angles, the propagation lengths of the $\pm m$-modes differ significantly, suggesting that the depth of the azimuthal intensity modulation decreases.

The permittivity of the nanowire, its radius and the permittivity of the outer medium may be potentially used for achieving the maximum rotation of the desired mode, but this question has not been investigated in details yet.

6 Topological plasmonics of the graphene-based meta-structures

As pointed above, replacing a continuous graphene layer by a periodic arrangement of graphene stripes (graphene meta-surface) may significantly affect the plasmonic properties of the structure. As we are going to show below, the transformation of the meta-surface topology (see Figure 8 for details) from a flat surface into a cylinder (meta-tube) and further into a torus (meta-torus) may lead to non-trivial change of plasmonic properties [57].

The transformation of a flat meta-surface in a meta-tube can only be achieved by a finite number of ways (see Figure 8A): the periodic boundary condition with respect to the azimuthal angle and the intrinsic periodicity of the meta-surface give rise to a set of discrete tilt angles:

$$\theta_n = \arcsin[n\Lambda / 2\pi r]. \tag{5}$$

An integer number n, to be denoted as the "topological index", is the number of graphene stripes winding around the meta-tube. It represents the topological index of the structure because under homeomorphic transformations, one cannot change the count of the spirals. The maximum topological index $n_{max} = 2\pi r/\Lambda$ corresponds to the longitudinal orientation of graphene stripes.

Similarly to the previous section, SPPs propagating along the cylindrical meta-tube are described by electric and magnetic fields $\mathbf{E_m}$, $\mathbf{H_m} \sim \exp[-i\omega t + ihz + im\varphi]$ and modes with opposite $\pm m$ propagate at different angles with respect to the graphene stripes in our chiral structure. Calculations show that propagation constants $h_\pm$ for these modes are different as well. We will focus on the modes with $m = \pm 1$ (to be denoted as $\sigma_\pm$ due to the analogy to the phenomenon of the Faraday rotation in bulk materials) and discuss their dispersion characteristics in detail.

In chiral structures, the wave vectors of σ_+ ($m=1$) and σ_- ($m=-1$) SPP-modes are oriented differently with respect to graphene stripes. This leads to the difference in their dispersion relation: whereas σ_+ SPPs possess a cut-off frequency of 10 THz, σ_- SPPs are allowed to propagate at lower frequencies. In other words, σ_+ and σ_- dispersion curves are characterized by slightly

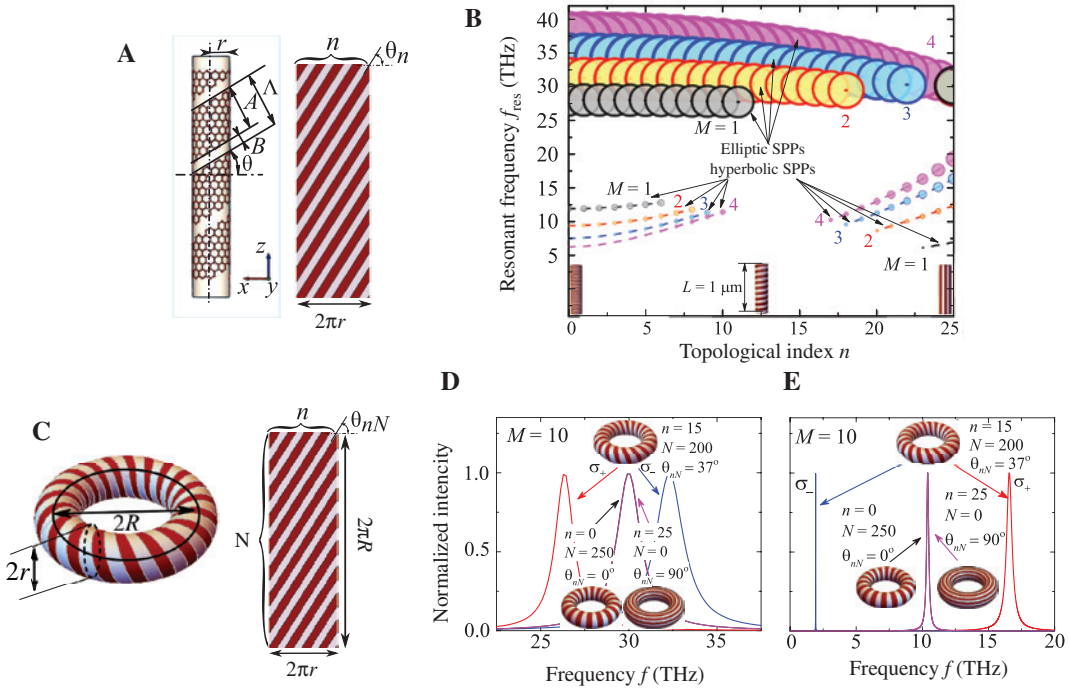

Figure 8: Topological transformations of nanostructures formed by meta-surfaces. A graphene-based meta-tube (A) is obtained by winding a bunch of n-identical graphene stripes around the cylindrical core under the fixed angle θ_n. The resonant frequencies of a finite-length meta-tube (B) depend on the topological index n. A graphene-based meta-torus (C) is obtained by bending a meta-tube in a donut: it is characterized by a pair of topological indexes n and N. Elliptic (D) and hyperbolic (E) σ_+ and σ_- SPP resonances on meta-tori with $M = 10$, $R/r = 10$ and different n and N; these resonances display a large spitting for a chiral structure ($n = 15$, $N = 200$) and are degenerate for the tori with perpendicular ($n = 0$) and parallel ($N = 0$) stripes (see text for details). Adapted from [57].

different bandgaps where SPPs cannot propagate. The bandgap opening is caused by the transition from the elliptic (above the bandgap) to the hyperbolic (below the bandgap) SPPs dispersion. This transition occurs at highly anisotropic σ-near-zero points of the metasurface, where their resonant response is accompanied by large dissipative losses. Obviously, the difference in bandgaps can be used to design structures for the asymmetric, one-way SPP propagation.

To justify the importance of $\sigma_\pm$ SPP modes, here we note that a linearly polarized electromagnetic wave impinging on the tip of our meta-tube at $z = 0$ will predominantly excite the linear combination of σ_+ and σ_- SPPs with equal amplitudes (i.e. the azimuthal field distribution $\cos[\varphi]$). The field distribution will rotate under a propagation similar to the graphene-covered magnetized nanowire considered in the previous section. Adjusting the graphene's chemical potential, though the external gate voltage or intrinsic chemical doping can significantly modify the specific rotation ψ_0. The maximum values of ψ_0 are expected to be much larger than those predicted in previous section for the gyrotropic graphene-covered nanowires under similar conditions.

An opposite chirality of the structure can be formally obtained either by assuming negative tilt numbers (or tilt angles) or backward propagating waves.

The asymmetric properties of the structure give the condition for the Fabry-Perot resonances in the finite length meta-tube $L[h_+(\omega_{res}) + h_-(\omega_{res})] = 2\pi M$, where M is an integer number. The resonant frequencies are shown in Figure 8B. Both hyperbolic (below the bandgap) and elliptic (above the bandgap) SPPs may form resonances. A significant shift of the cut-off frequencies for the forward- and backward-propagating SPPs may prohibit the existence of some lower-order Fabry-Perot modes in chiral meta-tubes because of the one-way propagation regime. For the higher-order Fabry-Perot resonances (large M), h increases and $\alpha_{\sigma\pm}$ both get close to 90° when the difference between two polarizations $\sigma_\pm$ ($m = \pm 1$) is negligible. This leads to the narrower range of parameters where the above-mentioned effect may be observed.

In the experiment, a linear combination of the fundamental mode ($m = 0$) and the chiral mode ($m = +1$ or $m = -1$) can be excited by a linearly polarized light beam focused under an appropriate angle on a tip of a silver

nanowire [106–108]. A similar excitation of a chiral meta-tube, with parameters corresponding to the one-way propagation regime, should lead to the creation of an electromagnetic "hotspot" at one of the tips [109]; for modes with an opposite chirality, the hotspot will be located at the opposite tip.

An even more interesting approach to change the topology of the structure is to transform a cylinder into a torus and thus introduce the second topological index N (see Figure 8C). In such a system, the tilt angle θ_{nN} must satisfy two distinct conditions: $\theta_{nN} = \arcsin[n\Lambda/2\pi r]$ and $\theta_{nN} = \arccos[N\Lambda/2\pi R]$. For an arbitrary geometry of the torus, these conditions are usually not satisfied for an all n. For example, two distinct configurations with perpendicular ($n=0$, $N=N_{max}$) and longitudinal ($n=n_{\max}$, $N=0$) orientations of the graphene stripes exist only if the ratio R/r of the torus radii is an integer.

The Fabry-Perot condition for modes propagating on a torus clockwise and counterclockwise ($2\pi Rh_{\pm}=2\pi M$) will be satisfied for two different frequencies. Only in two degenerate cases of 0° and 90° tilt angle would the mode propagation be symmetric and both resonant frequencies would become identical. The resonances of all orders exist in the meta-torus for all possible topological indexes in contrast to the finite length meta-tube. The resonant condition for the meta-torus $Rh=M$ uniquely defines the effective propagation angle of the SPPs: $\tan(\alpha_{mM}) = hr/m = Mr/mR$. In analogy to the topological indices n and N, a pair of electrodynamic indices m and M defines the electrodynamic topology of the resonant mode. The existence of topological SPP resonances on a meta-torus implies a fixed relation between the structural topological indices (n, N) and electromagnetic topological indices (m, M) of a resonant mode:

$$\frac{n}{N}\operatorname{ctg}\theta_{nN} = \frac{m}{M}\operatorname{tg}\alpha_{mM} \tag{6}$$

In general, elliptical and hyperbolic $\sigma_{\pm}$ modes possess different frequencies for all structures. An exception is an exotic case when SPP's propagation angle $\alpha_{\sigma\pm}=45°$ with respect to graphene stripes is identical for longitudinal and perpendicular stripe orientations. In this case, the splitting of resonant elliptic and hyperbolic $\sigma_{\pm}$ modes for a chiral structure is almost the largest one, and Eq. (6) helps explain such behavior. The analysis of SPPs propagating on a flat metasurface shows that their frequencies display the largest difference for wave vectors along and perpendicular with respect to graphene stripes, respectively. For resonant modes in the chiral toroidal resonator, we have equal $h_{\sigma\pm}$, and thus, $\alpha_{\sigma-}=180°-\alpha_{\sigma+}$. In analogy to planar metasurfaces, the maximum frequency splitting in chiral toroidal structure should be achieved for $\alpha_{\sigma-}-\alpha_{\sigma+}=90°$, which leads to $\alpha_{\sigma+}=45°$, $\alpha_{\sigma-}=135°$; in addition, we should have $\theta_{nN}=45°$. Under these conditions, we can use Eq. (6) to calculate the set of the topological indices for the maximum frequency splitting obeying $Mn/N=1$. The resonant curves in the vicinity to this condition are shown in Figure 8D and E.

7 Concluding remarks

We have reviewed the most recent results in plasmonics of magnetic and topological graphene-based nanostructures. The giant Faraday rotation of high-order plasmonic modes in graphene-covered nanowire and their tuning by both the gyrotropy (magnetic field or magnetization) and graphene chemical potential (chemical doping or gate voltage) may be used to magnetically control the density of states of electromagnetic radiation at the deeply subwavelength length scale, an effect interesting for quantum-optical devices operating in the telecom frequency range [110]. In nanowires of finite length, the magnetic field can be exploited to tune the Fabry-Perot cavity modes, an effect going beyond the resonant enhancement of Faraday rotation in the magneto-optical medium positioned inside an optical resonator [111].

While a graphene meta-tube displays a similar rotation of azimuthal plasmonic modes, the larger magnitude of the rotation per unit length plays a crucial role for the design of "one-way propagation" plasmonic devices: it is responsible for the disappearance of Fabry-Perot resonances in finite-length meta-tubes. A piece of a meta-tube, rolled in a torus, possesses a distinct spectrum of azimuthal cavity modes with an unexpectedly large energy splitting between the clockwise- and counterclockwise-propagating SPP modes. Interestingly, the electromagnetic and geometrical topological indices of the structure are intimately connected by simple analytical expressions, whose physical meaning remains to be clarified.

In this review, we have discussed two kinds of topology. The first one is the topology of the isofrequency contours (at one frequency) observed on hyperbolic graphene metasurfaces. The second one is a geometrical topology that characterizes the geometry of meta-cylinders and meta-tori. It is characterized by an integer topological index n, which determines the electromagnetic behavior of plasmons.

The third kind of topology, which we have not discussed in this review article, is related to the topology of the bands (several frequencies) over the entire Brillouin

zone. It is quantified by the so-called Chern number, whose change implies a topological phase transition that corresponds to drastic change in the physical properties of the system (see Ref. [112]). Recent investigations of the topological aspects of the third kind (i.e. Chern numbers, Berry phase, Berry connection etc.) of electromagnetic waves propagation in bianisotropic continuous media attracted considerable interest as well [113, 114]. For example, as the bulk transparent magneto-optical material is continuously transformed in isotropic opaque plasma, the evolution of band structure Chern numbers of individual electromagnetic modes experiences the jumps [114]. In another relevant example of SPPs propagating along the interface between an isotropic plasma and anisotropic (magneto-optical) dielectric material, one-way propagation of SPPs is found [114], whereas the propagation direction is uniquely determined by the direction of an external magnetic field. Such systems with broken time-reversal symmetry are sometimes designated as Chern-type insulators (the analogs of quantum Hall insulators). Some recent works have been devoted to the investigation of topologically protected (plasmonic) edge states in 2D materials and particularly graphene with the magnetically broken time reversal symmetry [115, 116].

It is worth mentioning that the interplay between the chirality and the hyperbolicity in bulk metamaterials quite similar to the system considered in previous section (see Figure 8A) may lead to the protection of the edge states from backscattering even without the requirement to break the time-reversal symmetry [117].

The similarity of the effects for magnetized and chiral graphene-based cylinders raises the question of the possibility of magnetic compensation of the chirality effect in hybrid magneto-chiral plasmonic structures (see Figure 9). The interplay between chirality and gyrotropy in magnetized chiral waveguides formed by plasmonic nano-ellipsoids has been shown to strongly enhance the nonreciprocal response of the structure [118]. In the

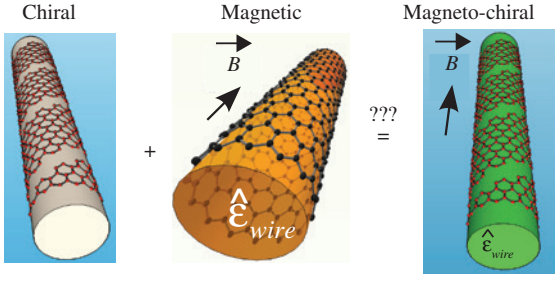

Figure 9: The concept of hybrid magneto-chiral nanostructures for possible non-reciprocal magnetic compensation of the chirality effects.

cylindrical geometry proposed here, we expect a non-trivial interference between the geometrical chirality and gyrotropy on SPPs with opposite electromagnetic chirality m. It might manifest itself in a different dependence of $h_+(B)$ and $h_-(B)$ on the amplitude B of the external magnetic field. The broken time-reversal symmetry can be achieved not only by magnetic effects discussed above but also through the optical pumping [119, 120].

Another open problem is the self-consistent propagation of high-intensity SPPs in systems with magneto-optical materials. Whereas the magnetization naturally affects the SPP characteristics via the (linear) magneto-optical effect, the SPPs may also affect the magnetization via inverse (nonlinear) magneto-optical effects. The inverse Faraday effect generates the magnetic field $\delta B(E) \sim E^2$ and introduces the nonlinear correction to the off-diagonal permittivity components:

$$\varepsilon_a \to \varepsilon_a + bE^2, \tag{7}$$

an effect similar to the third-order non-linearity is expected in Maxwell's equations [121]. The complexity of field distributions in cylindrical systems [103] makes it difficult to solve this problem analytically. However, this non-trivial possibility of combining transient magnetic effects with nonlinear optics, without using an external magnetic field, represents an interesting problem for computational electrodynamics.

An interesting perspective was provided by the possibility to apply external strains to meta-structures. Let us consider a non-chiral structure formed by a nanowire longitudinally covered by graphene stripes, where no rotation of high-order plasmonic modes can be observed. If shear strains are applied to such a structure, the spiral waveguide will be formed with the tilt angle defined by the strain value. Alternatively, an axial strain applied to the chiral structure will lead to a change in spacer width and the periodicity of the structure, or equivalently to change the filling factor. In any case, the rotation angle of the electromagnetic field distribution at the output of the meta-tube will be modified by the applied strain. For a finite-length meta-tube frequency of Fabry-Perot resonances, the frequency will be shifted or even some resonances may vanish. These effects may be useful for future applications as plasmonic strain sensors.

An even more intriguing effect of elastic deformations on plasmonic properties may be envisaged in spatially uniform graphene-based nanowires. We have pointed above that in cylindrical geometry, the intrinsic magneto-plasmonic properties of graphene cannot be used, because the radial magnetization is needed. However, it is

well known that external strains may affect the electronic properties of graphene similar to an external magnetic field (i.e. strains may induce the so-called pseudo-magnetic field) [122]. Thus, the investigation of acousto-magneto-plasmonic effects in graphene-based nanowires extends beyond the straightforward effects dominated by the influence of core magnetization on SPPs propagating along graphene nanowires.

Acknowledgments: The work was financially supported in part by RFBR (16-37-00023, 16-07-00751, 16-29-14045, 17-57-150001), RScF (14-22-00279), Grant of the President of the RF (MK-1653.2017.2), Act 211 Government of the Russian Federation (contract № 02.A03.21.0011), Stratégie internationale NNN-Telecom de la Région Pays de La Loire, PRC CNRS-RFBR "Acousto-magneto-plasmonics" and the PhOM Research Seminars Program of the Université Paris-Saclay.

References

[1] Bao Q, Loh KP. Graphene photonics, plasmonics, and broadband optoelectronic devices. ACS Nano 2012;6:3677.
[2] Grigorenko AN, Polini M, Novoselov KS. Graphene plasmonics. Nat Photonics 2012;6:749–58.
[3] de Abajo FJG. Graphene plasmonics: challenges and opportunities. ACS Photonics 2014;1:135.
[4] Huang S, Song C, Zhang G, Yan H. Graphene plasmonics: physics and potential applications. Nanophotonics 2016;6:1191.
[5] Chen P-Y, Argyropoulos C, Farhat M, Gomez-Diaz JS. Flatland plasmonics and nanophotonics based on graphene and beyond. Nanophotonics 2017;6:1239.
[6] Low T, Avouris P. Graphene plasmonics for terahertz to mid-infrared applications. ACS Nano 2014;8:1086.
[7] Low T, Chaves A, Caldwell JD, et al. Polaritons in layered two-dimensional materials. Nat Mater 2017;16:182.
[8] Mikhailov SA, Ziegler K. New electromagnetic mode in graphene. Phys Rev Lett 2007;99:016803.
[9] Hanson GW. Quasi-transverse electromagnetic modes supported by a graphene parallel-plate waveguide. J Appl Phys 2008;104:084314.
[10] Bludov YV, Ferreira A, Peres NMR, Vasilevskiy M. A primer on surface plasmon-polaritons in graphene. Int J Mod Phys B. 2013;27:1341001.
[11] Kotov OV, Kol'chenko MA, Lozovik YE. Ultrahigh refractive index sensitivity of TE-polarized electromagnetic waves in graphene at the interface between two dielectric media. Opt Express 2013;21:13533.
[12] Buslaev PI, Iorsh IV, Shadrivov IV, Belov PA, Kivshar YS. Plasmons in waveguide structures formed by two graphene layers. JETP Lett 2013;97:535.
[13] Smirnova DA, Iorsh IV, Shadrivov IV, Kivshar YS. Multilayer graphene waveguides. JETP Lett 2014;99:456.
[14] Lamata IS, Alonso-González P, Hillenbrand R, Nikitin AY. Plasmons in cylindrical 2D materials as a platform for nanophotonic circuits. ACS Photonics 2015;2:280.
[15] Kuzmin DA, Bychkov IV, Shavrov VG, Kotov LN. Transverse-electric plasmonic modes of cylindrical graphene-based waveguide at near-infrared and visible frequencies. Sci Rep 2016;6:26915.
[16] Gao Y, Ren G, Zhu B, Liu H, Lian Y, Jian S. Analytical model for plasmon modes in graphene-coated nanowire. Opt Express 2014;22:24322.
[17] Koppens FHL, Chang DE, de Abajo FJG. Graphene plasmonics: a platform for strong light-matter interactions. Nano Lett 2011;11:3370–7.
[18] Krasavin AV, Zheludev NI. Active plasmonics: controlling signals in Au/Ga waveguide using nanoscale structural transformations. Appl Phys Lett 2004;84:1416.
[19] Fedutik Y, Temnov VV, Schöps O, Woggon U, Artemyev MV. Exciton-plasmon-photon conversion in plasmonic nanostructures. Phys Rev Lett 2007;99:136802.
[20] Temnov VV, Armelles G, Woggon U, et al. Active magneto-plasmonics in hybrid metal-ferromagnet structures. Nat Photonics 2010;4:107.
[21] LeBlanc SJ, McClanahan MR, Jones M, Moyer PJ. Enhancement of multiphoton emission from single CdSe quantum dots coupled to gold films. Nano Lett 2013;13:1662.
[22] Abbasi F, Davoyan AR, Engheta N. One-way surface states due to nonreciprocal light-line crossing. New J Phys 2015;17:063014.
[23] Kurkin MI, Bakulina NB, Pisarev RV. Transient inverse Faraday effect and ultrafast optical switching of magnetization. Phys Rev B 2008;78:134430.
[24] Mentink JH, Hellsvik J, Afanasiev DV, et al. Ultrafast spin dynamics in multisublattice magnets. Phys Rev Lett 2012;108:057202.
[25] Kirilyuk A, Kimel AV, Rasing T. Laser-induced magnetization dynamics and reversal in ferrimagnetic alloys. Rep Prog Phys 2013;76:026501.
[26] Kurkin MI, Orlova NB. Femtosecond magnetooptics and ultrafast magnetization reversal of ferromagnetic. J Magn Magn Mater 2014;361:224.
[27] Belotelov VI, Doskolovich LL, Zvezdin AK. Extraordinary magneto-optical effects and transmission through metal-dielectric plasmonic systems. Phys Rev Lett 2007;98:077401.
[28] Jain PK, Xiao Y, Walsworth R, Cohen AE. Surface plasmon resonance enhanced magneto-optics (SuPREMO): Faraday rotation enhancement in gold-coated iron oxide nanocrystals. Nano Lett 2009;9:1644.
[29] Wang L, Yang K, Clavero C, et al. Localized surface plasmon resonance enhanced magneto-optical activity in core-shell Fe-Ag nanoparticles. J Appl Phys 2010;107:09B303.
[30] Belotelov VI, Akimov IA, Pohl M, et al. Enhanced magneto-optical effects in magnetoplasmonic crystals. Nat Nanotechnol 2011;6:370.
[31] Kreilkamp LE, Belotelov VI, Chin JY, et al. Waveguide-plasmon polaritons enhance transverse magneto-optical Kerr effect. Phys Rev X 2013;3:041019.
[32] Khokhlov NE, Prokopov AR, Shaposhnikov AN, et al. Photonic crystals with plasmonic patterns: novel type of the heterostructures for enhanced magneto-optical activity. J Phys D Appl Phys 2015;48:095001.
[33] Razdolski I, Makarov D, Schmidt OG, et al. Nonlinear surface magnetoplasmonics in Kretschmann multilayers. ACS Photonics 2016;3:179.

[34] Temnov VV. Ultrafast acousto-magneto-plasmonics. Nat Photonics 2012;6:728.
[35] Gomez-Diaz JS, Tymchenko M, Alù A. Hyperbolic metasurfaces: surface plasmons, light-matter interactions, and physical implementation using graphene stripes. Opt Mater Express 2015;5:246047.
[36] Gomez-Diaz JS, Tymchenko M, Alù A. Hyperbolic plasmons and topological transitions over uniaxial metasurface. Phys Rev Lett 2015;114:233901.
[37] Gomez-Diaz JS, Alù A. Flatland optics with hyperbolic metasurfaces. ACS Photonics 2016;3:2211.
[38] Schaferling M, Yin X, Engheta N, Giessen H. Helical plasmonic nanostructures as prototypical chiral near-field sources. ACS Photonics 2014;1:530.
[39] Engheta N, Pelet P. The theory of chirowaveguides. IEEE Trans Microwave Theory Tech 1990;38:1631.
[40] Jaggard DL, Engheta N, Kowarz MW, Pelet P, Liu JC, Kim Y. Periodic chiral structures. IEEE Trans Antennas Propag 1989;37:1447.
[41] Fedotov VA, Mladyonov PL, Prosvirnin SL, Rogacheva AV, Chen Y, Zheludev NI. Asymmetric propagation of electromagnetic waves through a planar chiral structure. Phys Rev Lett 2006;97:167401.
[42] Pendry JB. A chiral route to negative refraction. Science 2004;306:1353.
[43] Baranova NB, Zel'dovich BY. Rotation of a ray by a magnetic field. JETP Lett 1994;59:681.
[44] Darsht MY, Zhirgalova IV, Zel'dovich BY, Kundikova ND. Observation of a "magnetic" rotation of the speckle of light passed through an optical fiber. JETP Lett 1994;9:763.
[45] Ardasheva LI, Sadykova MO, Sadykov NR, et al. Rotation of the speckle pattern in a low-mode optical fiber in a longitudinal magnetic field. J Opt Technol 2002;69:451.
[46] Ardasheva LI, Kundikova ND, Sadykova MO, Sadykov NR, Chernyakov VE. Speckle-pattern rotation in a few-mode optical fiber in a longitudinal magnetic field. Opt Spectrosc 2003;95:645.
[47] Kuzmin DA, Bychkov IV, Shavrov VG. Influence of graphene coating on speckle-pattern rotation of light in gyrotropic optical fiber. Opt Lett 2015;40:890.
[48] Kuzmin DA, Bychkov IV, Shavrov VG, Temnov VV. Giant Faraday rotation of high-order plasmonic modes in graphene-covered nanowires. Nano Lett 2016;16:4391.
[49] Kort-Kamp WJM, Rosa FSS, Pinheiro FA, Farina C. Tuning plasmonic cloaks with an external magnetic field. Phys Rev Lett 2013;111:215504.
[50] Kort-Kamp WJM, Rosa FSS, Pinheiro FA, Farina C. Molding the flow of light with a magnetic field: plasmonic cloaking and directional scattering. J Opt Soc Am A 2014;31:1969.
[51] Wang Z, Fan S. Optical circulators in two-dimensional magneto-optical photonic crystals. Opt Lett 2005;30:1989.
[52] Smigaj W, Romero-Vivas J, Gralak B, Magdenko L, Dagens B, Vanwolleghem M. Magneto-optical circulator designed for operation in a uniform external magnetic field. Opt Lett 2010;35:568.
[53] Dmitriev V, Kawakatsu MN, Portela G. Magneto-optical resonator switches in two-dimensional photonic crystals: geometry, symmetry, scattering matrices, and two examples. Opt Lett 2013;38:1016.
[54] Falk AL, Chiu K-C, Farmer DB, et al. Coherent plasmon and phonon-plasmon resonances in carbon nanotubes. Phys Rev Lett 2017;118:257401.
[55] Kim C-J, Sánchez-Castillo A, Ziegler Z, et al. Chiral atomically thin films. Nature Nanotechnol 2016;11:520.
[56] Stauber T, Low T, Gómez-Santos G. Chiral response of twisted bilayer graphene. 2017; arXiv:1708.06116.
[57] Kuzmin DA, Bychkov IV, Shavrov VG, Temnov VV. Topologically induced optical activity in graphene-based meta-structures. ACS Photonics 2017;4:1633.
[58] Zheng Y, Ando T. Hall conductivity of a two-dimensional graphite system. Phys Rev B 2002;65:245420.
[59] Gusynin VP, Sharapov SG. Unconventional integer quantum Hall effect in graphene. Phys Rev Lett 2005;95:146801.
[60] Castro Neto AH, Guinea F, Peres NMR. Edge and surface states in the quantum Hall effect in graphene. Phys Rev B 2006;73:205408.
[61] Sheng DN, Sheng L, Weng ZY. Quantum Hall effect in graphene: disorder effect and phase diagram. Phys Rev B 2006;73:233406.
[62] Abanin DA, Lee PA, Levitov LS. Spin-filtered edge states and quantum Hall effect in graphene. Phys Rev Lett 2006;96:176803.
[63] Lukose V, Shankar R, Baskaran G. Novel electric field effects on Landau levels in graphene. Phys Rev Lett 2007;98:116802.
[64] Zhang Y, Tan Y-W, Stormer HL, Kim P. Experimental observation of the quantum Hall effect and Berry's phase in graphene. Nature (London) 2005;438:201.
[65] Novoselov KS, McCann E, Morozov SV, et al. Unconventional quantum Hall effect and Berry's phase of 2π in bilayer graphene. Nat Phys 2002;2:177.
[66] Zhang Y, Jiang Z, Small JP, et al. Landau-level splitting in graphene in high magnetic fields. Phys Rev Lett 2006;96:136806.
[67] Novoselov KS, Geim AK, Morozov SV, et al. Two-dimensional gas of massless Dirac fermions in graphene. Nature 2005;438:197.
[68] Sharapov SG, Gusynin VP, Beck H. Magnetic oscillations in planar systems with the Dirac-like spectrum of quasiparticle excitations. Phys Rev B 2004;69:075104.
[69] Sharapov SG, Gusynin VP. Magnetic oscillations in planar systems with the Dirac-like spectrum of quasiparticle excitations II: transport properties. Phys Rev B 2005;71:125124.
[70] Nair RR, Blake P, Grigorenko AN, et al. Fine structure constant defines visual transparency of graphene. Science 2008;320:1308.
[71] Li ZQ, Henriksen EA, Jiang Z, et al. Dirac charge dynamics in graphene by infrared spectroscopy. Nat Phys 2008;4:532.
[72] Mak KF, Sfeir MY, Wu Y, et al. Measurement of the optical conductivity of graphene. Phys Rev Lett 2008;101:196405.
[73] Falkovsky LA, Pershoguba SS. Optical far-infrared properties of graphene monolayer and multilayers. Phys Rev B 2007;76:153410.
[74] Stauber T, Peres NMR, Geim AK. Optical conductivity of graphene in the visible region of the spectrum. Phys Rev B 2008;78:085432.
[75] Kuzmenko AB, van Heumen E, Carbone F, van der Marel D. Universal optical conductance of graphite. Phys Rev Lett 2008;100:117401.
[76] Falkovsky LA, Varlamov AA. Space-time dispersion of graphene conductivity. Eur Phys J B 2007;56:281.
[77] Hanson GW. Dyadic Green's functions for an anisotropic, nonlocal model of biased graphene. IEEE Trans Antennas Propag 2008;56:747.

[78] Gusynin VP, Sharapov SG, Carbotte JP. Sum rules for the optical and Hall conductivity in graphene. Phys Rev B 2007;75:165407.
[79] Gusynin VP, Sharapov SG, Carbotte JP. Unusual microwave response of Dirac quasiparticles in graphene. Phys Rev Lett 2006;96:256802.
[80] Dean CR, Young AF, Meric I, et al. Boron nitride substrates for high-quality graphene electronics. Nat Nanotechnol 2010;5:722.
[81] Crassee I, Levallois J, Walter AL, et al. Giant Faraday rotation in single- and multilayer graphene. Nat Phys 2010;7:48.
[82] Shimano R, Yumoto G, Yoo JY, et al. Quantum Faraday and Kerr rotations in graphene. Nat Commun 2013;4:1841.
[83] Sounas DL, Skulason HS, Nguyen HV, et al. Faraday rotation in magnetically biased graphene at microwave frequencies. Appl Phys Lett 2013;102:191901.
[84] Falkovsky LA. Quantum magneto-optics of graphite with trigonal warping. Phys Rev B 2011;84:115414.
[85] Gusynin VP, Sharapov SG, Carbotte JP. Magneto-optical conductivity in graphene. J Phys Condens Matter 2007;19:026222.
[86] Ferreira A, Peres NMR, Castro Neto AH. Confined magneto-optical waves in graphene. Phys Rev B 2012;85:205426.
[87] Iorsh IV, Shadrivov IV, Belov PA, Kivshar YS. Tunable hybrid surface waves supported by a graphene layer. JETP Lett 2013;97:249.
[88] Melo LGC. Theory of magnetically controlled low-terahertz surface plasmon-polariton modes in graphene-dielectric structures. J Opt Soc Am B 2015;32:2467.
[89] Yan H, Li Z, Li X, Zhu W, Avouris P, Xia F. Infrared spectroscopy of tunable Dirac terahertz magneto-plasmons in graphene. Nano Lett 2012;12:3766.
[90] Crassee I, Orlita M, Potemski M, et al. Intrinsic terahertz plasmons and magnetoplasmons in large scale monolayer graphene. Nano Lett 2012;12:2470.
[91] Berman OL, Gumbs G, Lozovik YE. Magnetoplasmons in layered graphene structures. Phys Rev B 2008;78:085401.
[92] Sounas DL, Caloz C. Edge surface modes in magnetically biased chemically doped graphene stripes. Appl Phys Lett 2011;99:231902.
[93] Tymchenko M, Nikitin AY, Martín-Moreno L. Faraday rotation due to excitation of magnetoplasmons in graphene microribbons. ACS Nano 2013;7:9780.
[94] Mast DB, Dahm AJ, Fetter AL. Observation of bulk and edge magnetoplasmons in a two-dimensional electron fluid. Phys Rev Lett 1985;54:1706.
[95] Wang W, Apell SP, Kinaret JM. Edge magnetoplasmons and the optical excitations in graphene disks. Phys Rev B 2012;86:125450.
[96] Kumada N, Roulleau P, Roche B. Resonant edge magnetoplasmons and their decay in graphene. Phys Rev Lett 2014;113:266601.
[97] Chamanara N, Sounas D, Caloz C. Non-reciprocal magnetoplasmon graphene coupler. Opt Express 2013;21:11248.
[98] Chamanara N, Sounas D, Szkopek T, Caloz C. Terahertz magnetoplasmon energy concentration and splitting in graphene PN junctions. Opt Express 2013;21:25356.
[99] Liu F, Qian C, Chong YD. Directional excitation of graphene surface plasmons. Opt Express 2015;23:2383.
[100] Nasari H, Abrishamian MS. Magnetically tunable focusing in a graded index planar lens based on graphene. J Opt 2014;16:105502.
[101] Kuzmin DA, Bychkov IV, Shavrov VG. Magnetic field control of plasmon polaritons in graphene-covered gyrotropic planar waveguide. Opt Lett 2015;40:2557.
[102] Kuzmin D, Bychkov I, Shavrov V. Electromagnetic waves absorption by graphene magnetic semiconductor multilayered nanostructure in external magnetic field: Voight geometry. Acta Phys Polon A 2015;127:528.
[103] Kuzmin DA, Bychkov IV, Shavrov VG, Temnov VV, Lee H-I, Mok J. Plasmonically induced magnetic field in graphene-coated nanowires. Opt Lett 2016;41:396.
[104] Martín-Becerra D, Temnov VV, Thomay T, et al. Spectral dependence of the magnetic modulation of surface plasmon polaritons in noble/ferromagnetic/noble metal films. Phys Rev B 2012;86:035118.
[105] Thongrattanasiri S, Manjavacas A, García de Abajo FJ. Quantum finite-size effects in graphene plasmons. ACS Nano 2012;6:1766.
[106] Zhang S, Wei H, Bao K, Håkanson U, Halas NJ, Nordlander P, Xu H. Chiral surface plasmon polaritons on metallic nanowires. Phys Rev Lett 2011;107:096801.
[107] Li Zh, Bao K, Fang Y, Huang Y, Nordlander P, Xu H. Correlation between incident and emission polarization in nanowire surface plasmon waveguides. Nano Lett 2010;10:1831.
[108] Wei H, Pana D, Xu H. Routing of surface plasmons in silver nanowire networks controlled by polarization and coating. Nanoscale 2015;7:19053.
[109] Chettiar UK, Davoyan AR, Engheta N. Hotspots from nonreciprocal surface waves. Opt Lett 2014;39:1760.
[110] Gao J, Fidler AF, Klimov VI. Carrier multiplication detected through transient photocurrent in device-grade films of lead selenide quantum dots. Nat Commun 2015;6:8185.
[111] Rosenberg R, Rubinstein CB, Herriott DR. Resonant optical Faraday rotator. Appl Opt 1964;3:1079.
[112] Silveirinha MG. Bulk-edge correspondence for topological photonic continua. Phys Rev B 2016;94:205105.
[113] Gangaraj SAH, Silveirinha MG, Hanson GW. Berry phase, Berry connection, and Chern number for a continuum bianisotropic material from a classical electromagnetics perspective. IEEE J Multiscale Multiphys Comput Technol 2017;2:3.
[114] Silveirinha MG. Chern invariants for continuous media. Phys Rev B 2015;92:125153.
[115] Jin D, Lu L, Wang Z, et al. Topological magnetoplasmon. Nat Commun 2016;7:13486.
[116] Jin D, Christensen T, Soljačić M, et al. Infrared topological plasmons in graphene. Phys Rev Lett 2017;118:245301.
[117] Gao W, Lawrence M, Yang B, et al. Topological photonic phase in chiral hyperbolic metamaterials. Phys Rev Lett 2015;114:037402.
[118] Hadad Y, Steinberg BZ. Magnetized spiral chains of plasmonic ellipsoids for one-way optical waveguides. Phys Rev Lett 2010;105:233904.
[119] Kumar A, Nemilentsau A, Fung KH, et al. Chiral plasmon in gapped Dirac systems. Phys Rev B 2016;93:041413.
[120] Songa JCW, Rudner MS. Chiral plasmons without magnetic field. Proc Natl Acad Sci USA 2015;113:4658.
[121] Im S-J, Ri C-S, Ho K-S, Herrmann J. Third-order nonlinearity by the inverse Faraday effect in planar magnetoplasmonic structures. Phys Rev B 2017;96:165437.
[122] Levy N, Burke SA, Meaker KL, et al. Strain-induced pseudo-magnetic fields greater than 300 tesla in graphene nanobubbles. Science 2010;329:544.